RESEARCH ARTICLE

Optimal Design of SPMSM for UAV Using Adjusted Evolution Strategy

JUNG-WOO KIM [1], **CHUL YUN** [2], **TAE-HO OH** [2], **DONG-KUK LIM** [1], (Member, IEEE), **AND JIN-HWAN LEE** [3]

[1]Department of Electrical, Electronic and Computer Engineering, University of Ulsan, Ulsan 44610, Republic of Korea
[2]Advanced Control Development Team 1, Research and Development Center, DN Solutions, Changwon-si 51537, Republic of Korea
[3]Department of Electrical Engineering, Chonnam National University, Gwangju 61186, Republic of Korea

Corresponding author: Jin-Hwan Lee (jh.lee@jnu.ac.kr)

ABSTRACT This paper proposes the optimization algorithm, an adjusted evolution strategy (AES) and verifies performance of the AES applying the optimal design of the outer-rotor surface mounted permanent magnet synchronous motor (SPMSM) for unmanned aerial vehicle. The proposed algorithm improved disadvantage of the conventional evolution strategy, which requires long computation time when solving the optimization problem, utilizing an exponential function of the annealing factor. In addition, the AES further enhances the convergence characteristic by combining with the compass segment method which is deterministic algorithm. This paper shows that the superiority of AES over NGA and ES in three test functions, with 30% to 70% reduction in the number of function calls, and an improvement of 5%p to 30%p in the convergence accuracy. Finally, the AES is applied to the optimization design of the outer-rotor SPMSM, and this paper derived the optimal model of the SPMSM to increase average torque and reduce torque ripple that causes vibration in unmanned aerial vehicle. As a result, proposed algorithm successfully derived the optimal model and verified the robustness. Therefore, the results of this study are expected to be widely applied to the multimodal optimization problem of various electrical machines utilizing FEM.

INDEX TERMS Design optimization, multi-modal optimization, unmanned aerial vehicle, motor design, surface mounted permanent magnet synchronous motor.

I. INTRODUCTION

Unmanned aerial vehicle (UAV) is in the spotlight around the world as a mobility option for the future. Various types of UAVs have been developed to solve complicated and dangerous missions safely and quickly, such as data acquisition, forest fire detection, and rescue and search missions [1], [2]. IT companies such as Google and Amazon also developed the first UAVs, starting with microdrones [3]. It is expected that many companies will be interested in the UAV industry in the future.

Systems of the UAV generally operate by motors [4]. The motor should have the features of tight structure and

The associate editor coordinating the review of this manuscript and approving it for publication was Deepak Mishra.

light weight for saving the space and mass, and it needs the high output density under high-speed-operation [5], [6], [7]. Permanent magnet synchronous motor (PMSM) among several motors is usually utilized for the UAV because it has high performances such as high efficiency, power density, ratio of output torque to motor weight, reliability, and high dynamic response performance [3], [8]. PMSMs are categorized as interior PMSM (IPMSM) or surface mounted PMSM (SPMSM) according to position of the permanent magnet. The SPMSM is relatively simple to control compared to the IPMSM. Which of the SPMSMs, outer-rotor SPMSM has large inertia than inner-rotor SPMSM [9], [10]. Therefore, outer-rotor SPMSM usually shows constant speed operation rather than acceleration operation [3]. Due to these characteristics, the outer-rotor SPMSM is usually used for UAVs

TABLE 1. Result according to annealing factor.

Annealing factor	Number of function calls	Success rate [%]
0.4	760	88.16
0.6	991	89.34
0.8	1545	91.07
0.85	2095	92.04
0.9	2704	93.14

TABLE 2. Result according to number of elite sets.

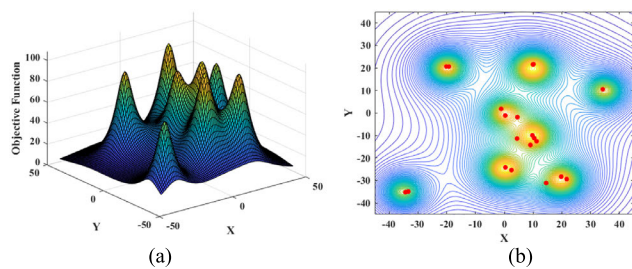| Number of elite sets	Number of function calls	Success rate [%]
5	418	44.54
10	893	73.20
15	1520	85.62
20	2358	93.47
25	3595	95.79

FIGURE 1. Problem areas having 8 peaks of the test functions and result using evolution strategy. (a) test function (b) result.

that require long take-off and stable operation. However, in the performances of the motor, cogging torque and torque ripple generate noise, and vibration and reduce efficiency of the motor. Therefore, reducing these performances through optimization is essential.

Finite element method (FEM) is used to accurately derive the performance of the SPMSM. which has non-linear magnetic saturation [12].

However, the FEM for the optimal design of the SPMSM having the nonlinear characteristic requires a lot of time [13], [14]. To resolve this problem, several algorithms finding the optimal design such as evolution strategy (ES) and niching genetic algorithm, which is multi-modal algorithm, have studied [15], [16], [17], [18], [19], [20], [21].

Multi-modal algorithm can find local peak and global peak [22], [23], [24], [25], [26], [27], [28]. Local peak refers to the most optimal solution among the surrounding solutions at the current location in an optimization problem. In other words, it is the optimal value in a specific area and the point where changes in that area do not improve anymore. Therefore, several local peaks can exist in problem area. And global peak represents the most optimal solution in problem area. Multi-modal algorithm in motor design is used a lot because it can be considered other electromagnetic characteristics such as rated torque and output in addition to the objective function [29], [30]. Among them, ES and NGA
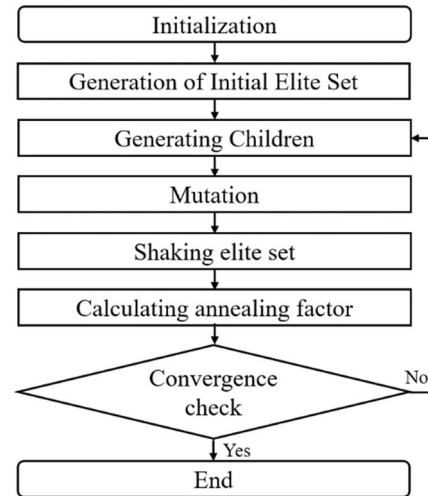

FIGURE 2. Flow chart of evolution strategy.

have superior detection of local peak capabilities compared to other multi-modal algorithms. Many studies are being conducted to improve the ES and NGA [12], [31]. However, in recent studying, the ES has problems about convergence characteristic, which is the accuracy with the peak in the nonlinearity problem area, and NGA also has problem that some peaks are difficult to find. And it occurs a lot of function calls, which are the number of times calculated to find a peak point in an unknown problem area, because elite range is decided without considering the number of surrounding samples [32]. Therefore, this study proposes the adjusted evolution strategy (AES) that applies exponentiation of the annealing factor that varies depending on the surrounding sample. And the AES adds some additional method to reduce function calls and the deterministic method, compass segment method (CSM), to enhance convergence characteristics. The proposed algorithm confirms superiority of function calls and accuracy through comparison of performance, while using the three mathematical test functions. In addition, the reliability of the proposed method was verified by successfully deriving the optimal design of SPMSM for UAVs.

In this paper, some methods which are applied to the proposed algorithm is described in section II. Subsequently, verification and comparison with the AES, the conventional ES, and NGA which is used a lot [33], are shown in section III. In section IV, V, this study selected design variables to optimize the target motor and finds the optimal design for the outer-rotor SPMSM with reduced torque ripple and increased average torque using the proposed algorithm. And to verify the stability of the motor, optimal model of the SPMSM for the UAV is proved stability about irreversible demagnetization of magnet.

II. PROPOSED ALGORITHM
The ES requires a lot of time to converge on peak points and has inferior convergence characteristic. Because the annealing factor which affects for deciding function calls
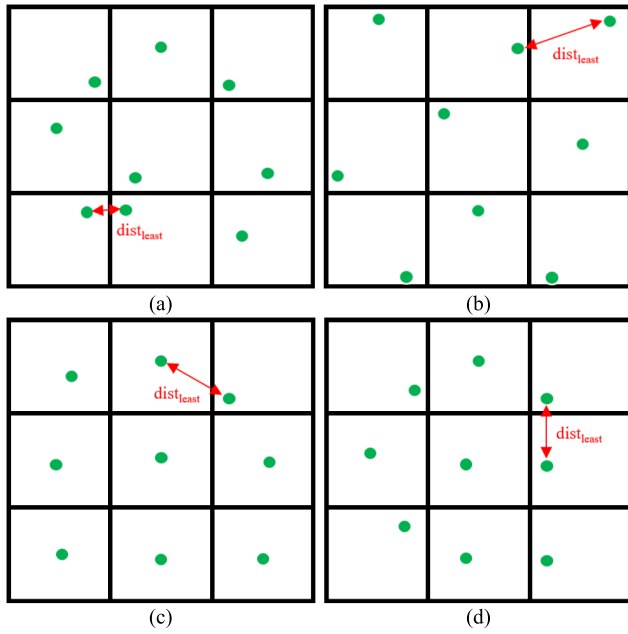
FIGURE 3. Groups of sample arrangement generated by the LHS. (a) group 1. (b) group 2. (c) group 3. (d) group 4.

and accuracy is fixed at 0.85 [34]. Therefore, while adding some methods which reduce function calls and enhance convergence characteristic, this paper proposes the AES using exponentializing of the annealing factor, restricted area, and deterministic method, CSM. As shown as Fig. 2, a description of the conventional ES, and characteristics of the upgraded ES are as follows [30].

A. CONVENTIONAL ALGORITHM-ES
ES is one of the basic algorithms, which have developed such as GA and simulated annealing (SA). The ES basically performs arithmetic optimization of real number functions and uses arithmetic operations not centered on the pattern but on the numbers themselves [35], [36], [37]. To obtain the optimal value, The elite set is determined by calculating the fitness of each particle as follow

$$F_i = (C_w - C_i) + \frac{C_w - C_b}{k - 1} \quad (1)$$

where C_w, C_b, and C_i are the minimum, maximum, and the i_{th} value of the cost functions, respectively. The value k is a number greater than 1, usually 3 or 4. After fitness determination, the k value is applied to the evolved solution-selected method such as roulette wheel or tournament. And then, the annealing factor is used to find the optimal value in the problem area while reducing the size of the elite set. The evolution range is updated by the annealing factor as follow

$$R_{i+1} = R_i \times \alpha \quad (2)$$

where R_i is the evolution range of the elite set, α is the annealing factor, and R_{i+1} is the evolved range. The annealing factor have a significant impact on the calculation time and

accuracy. Therefore, to confirm the function calls and accuracy according to the annealing factor, this paper utilizes the test function. The test function is defined as follow

$$f(x, y) = \sum_{i=1}^{P} \frac{m_i}{1 + [(x - x_i)^2 + (y - y_i)^2/n_i]} \quad (3)$$

where P is the size of the peak points of each test functions, and m_i and n_i determine the magnitude of each peak point. Table 1 shows the function calls and success rate by annealing factor in the test function of Fig. 1. (a) having 8 peaks. Success rate is the average of the absolute error for each peak. It is used for comparing performance of the convergence in terms of statistical indicators. The accuracy is calculated as follow

$$\text{Success rate}[\%] = \frac{(1 - |z_i - y_i|)}{n} \times 100 \quad (i = 1, 2, \cdots) \quad (4)$$

where n is the number of the peak, z_i is the i_{th} real peak of test function and y_i is the i_{th} peak found using optimization algorithm. Results in the Table 1 shows the smaller is the variable values, the faster the calculation time, but the lower the accuracy. In the most of algorithms using the ES, the annealing factor is fixed at 0.85 [34] with appropriate function calls, and accuracy.

B. PROPOSED ALGORITHM-AES
The conventional ES takes a lot of time to find optimal values and has bad convergence characteristic, as shown in Fig. 1. (b). To improve this characteristic, while generating the restricted area, changing the annealing factor, and combining the deterministic algorithm, the AES reduces the function calls and increases accuracy. The characteristics of the upgraded ES and the flow of the proposed algorithm are as follows.

1) IMPROVE LATIN HYPERCUBE SAMPLING
Generating initial samples evenly in the problem area is important because the location of the optimal solution in the problem area does not know. Nowadays, most of the algorithms generate initial samples by using Latin hypercube sampling (LHS) which is known for generating evenly. The LHS is a method for scattering initial samples evenly by considering the distance between each sample. And improved Latin hypercube sampling (ILHS) uses the LHS and is shown in Fig. 3. Groups of the initial samples are represented as Fig. 3 while using the LHS. The dist$_{least}$ in Figs. 3 is the smallest distance of the Euclidean distances between each sample in each group. And if the dist$_{least}$ is the largest of all the groups, the group is selected as the initial group [38]. This means that generating the using the ILHS increases the probability generating initial samples evenly than using the LHS. Therefore, this paper generates the initial samples using the ILHS.

(a)

(b)
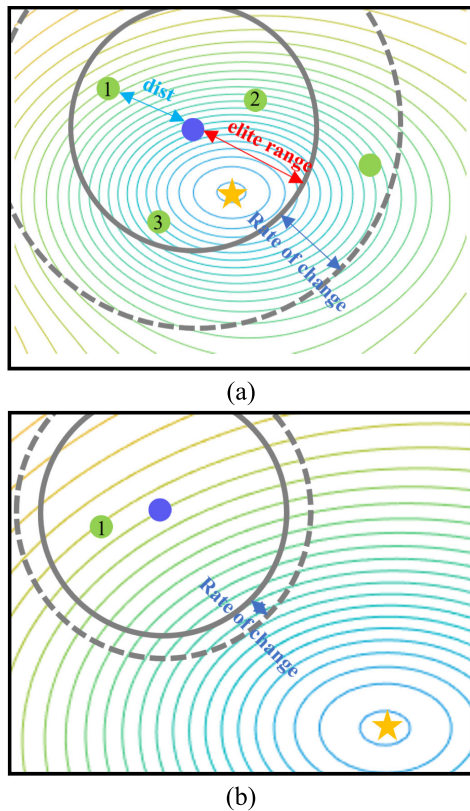
● : elite solution   ○ : elite set
● : non-elite solution   ⋰ : elite set by annealing
★ : optimal solution

FIGURE 4. Exponentialize the annealing factor utilizing of non-elite solutions in elite set. (a) part 1. (b) part 2.

2) EXPONENTIALIZE THE ANNEALING FACTOR

The annealing factor is the most important component of the ES. Annealing is a step which the probability of generating worse solutions decreases as the search progresses. Therefore, according to the annealing factor, the number of function calls and convergence accuracy are determined. The larger the annealing factor, the larger the rate of change in the evolution range, the faster the convergence speed, but the convergence accuracy decreases. On the contrary, as the annealing factor decreases, the rate of change in the evolution range decreases, and the convergence accuracy increases, but the convergence speed decreases. In the conventional ES, the annealing factor is fixed at 0.85 [34]. Hence, the function calls and accuracy of convergence are ambiguous because it does not consider the number of surrounding samples and is fixed value during the algorithm execution. To solve this problem, this paper proposes an exponential function of the annealing factor. As shown in Fig. 4, the annealing factor is exponentialized using surrounding samples to change the size of the elite set depending on the number of surrounding samples. The formula is as follow

$$AF = e^{-0.85f}(f = 1, 2, 3 \cdots) \tag{5}$$

(a)   (b)
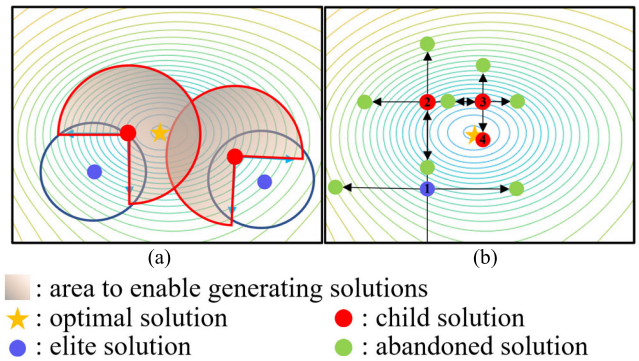
▨ : area to enable generating solutions
★ : optimal solution   ● : child solution
● : elite solution   ● : abandoned solution

FIGURE 5. Additional methods of the proposed algorithm which are different from conventional evolution strategy. (a) Restricted Area. (b) Compass Segment Method (CSM).

where AF is the annealing factor, f is the density factor using the number of other samples in the elite set and size of the objective function, and z is the objective function. Therefore, as repeating until the algorithm stops, the change in the size of the evolution range becomes more distinct compared to that of the conventional ES. Therefore, overlap is reduced, and function calls decrease by reducing unnecessary analysis.

3) RESTRICTED AREA & COMPASS SEGMENT METHOD

The AES utilizes a restricted area to increase the probability of achieving the superior solution. Restricted area is an area that excludes the area where the worse solution exists [39]. If the fitness of solutions in the elite range is elite solution, elite solutions are changed, existing elite solutions are deleted, and restricted areas are generated in that direction. Fig. 5. (a) shows the method of the restricted area. Therefore, setting the restricted area increases the probability of generating a better solution as the search progresses.

And the compass segment method (CSM) is the deterministic algorithm to develop the convergence characteristic of the AES. This generates solutions at the same length in four directions. After estimating the fitness of the four solutions, except for the best, everything else will be deleted. Reducing the length gradually, this process repeats until it finds the peak point. Fig. 5. (b) shows an example of the CSM.

4) FLOW CHART

The flow chart of the AES is shown in Fig. 6. First, initialization is a step which decide component of the AES like elite set, the number of initial samples, design variables, and so on. As shown in Table 2, the number of elite sets is fixed at 20 in considering rate of the increase in the success rate compared to the increase in the function call. And then, initial samples are generated evenly over the entire objective function region using the ILHS, and the fitness of each solution is calculated. And then, solutions having the high fitness are selected as the elite set, which is determined based on the following rules [34]

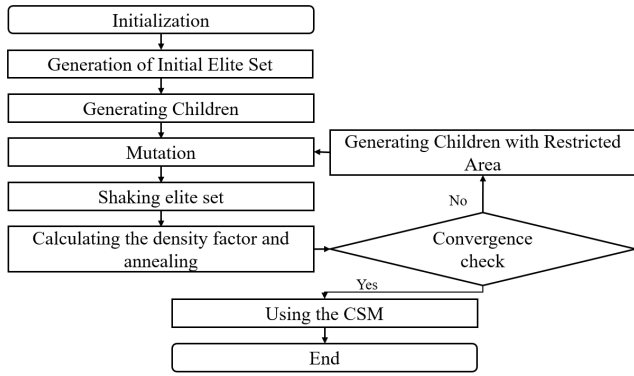A. Add a current best solution into the elite set and remove other solutions inside the evolution range.

FIGURE 6. Flow chart of adjusted evolution strategy.

B. Find another best solution and repeat the previous step. a specified number of times.

Next, create new child solutions within the mutation range of each elite solution (after repeating once, a child solution is generated in the elite set after exclusion of the restricted area). If a new child solution is improved compared to its parent, the existing solution is replaced by the child solution and the area is restricted further. If each elite solution is located in the evolution range of another solution, choose a good solution and remove a worse solution. Repeat this until the initial number of elite sets is reached. Next, mutated children are generated using LHS in the whole search space. If a mutation is better than an elite solution, the elite solution is replaced. If the mutation is in the evolution range, the range is increased by dividing by the annealing factor. However, if the elite solution is not replaced, the evolution range is decreased by multiplying by the annealing factor. This process is repeated until the average of respectively elite ranges is under the initial elite range. And then, to derive the optimal solution, the AES uses a deterministic method CSM that increases the convergence characteristic without probabilistic methods to reduce unnecessary analysis.

III. VERIFICATION OF THE PROPOSED ALGORITHM

To verify the performance of the proposed algorithm, the AES, the conventional optimization algorithm, ES, and NGA, are applied to the three mathematical test functions with 6 peaks, 10 peaks and 4 peaks, respectively. The test function 1 and 2 are defined as (3). And the test function 3 is as follow, meaning A is the magnitude of the peak.

$$f(x, y) = 2A + x^2 - A\cos(2\pi x) + y^2 - A\cos(2\pi y) \quad (6)$$

The test was performed 100 times with each algorithm. As shown in Table 3, the AES shows better performance than the NGA and the ES. Fig. 7. (a), (c), and (e) show problem area of the test functions 1, 2 and 3. They have 10 peaks, 6 peaks, and 4 peaks with certain locations and values. The test was conducted using the functions, was repeated 100 times, and was considered successful if the value of the peak was greater than 95 % of the actual peak value.
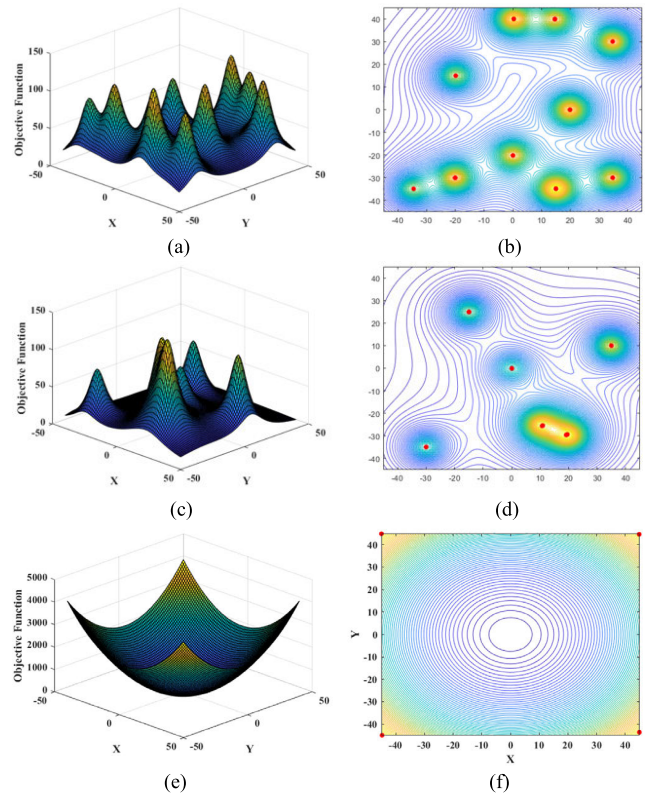

FIGURE 7. Problem areas and result of the test. (a) problem area of test function 1 (10 peaks). (b) result of test function 1 using the AES (10 peaks). (c) problem area of test function 2 (6 peaks). (d) result of test function 2 using the AES (6 peaks). (e) problem area of test function 3 (4 peaks), (f) result of test function 3 using the AES (4 peaks).

TABLE 3. Comparison of adjusted evolution strategy and niching algorithm for test functions.

10 peaks	Number of function calls	Success rate [%]
NGA	2040	81.43
ES	4343	94.28
AES	1150	99.85
6 peaks	Number of function calls	Success rate [%]
NGA	1040	73.68
ES	2305	92.92
AES	735	99.03
4 peaks	Number of function calls	Success rate [%]
NGA	540	69.99
ES	1063	86.09
AES	315	99.26

As shown in Fig. 7. (b), (d) and (f), the results are shown in Table 3 when all peaks are found in each test function. For the number of function calls and success rate, the first test function with 10 peaks showed a 99.85 % success rate in 1,150 function calls with the AES, an 81.43 % success rate in 2,040 function calls with the NGA, and a 93.70 % success rate in 2131 function calls with the ES. Likewise, with the second test function with 6 peaks, the AES showed a 99.03 % success rate in 735 function calls, while the NGA

TABLE 4. Specifications of the SPMSM for UAV.

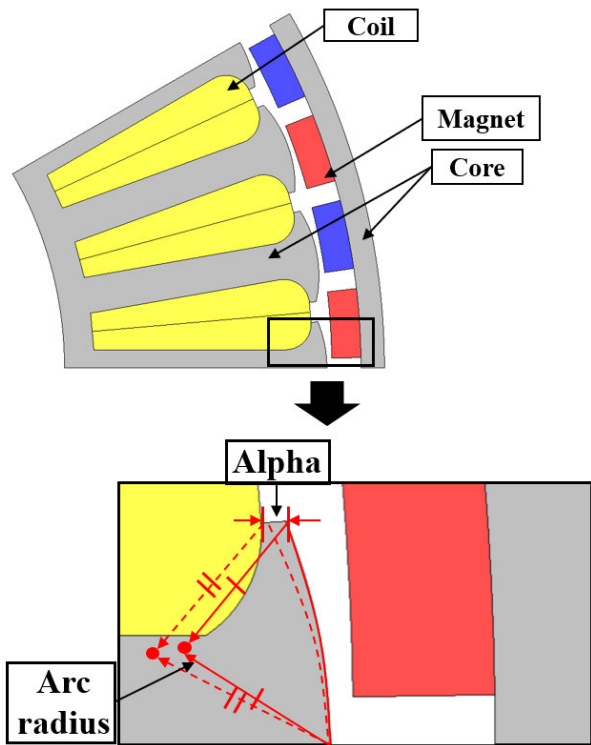| Specification	Value	Unit
Pole / Slot	48 / 36	-
Stator diameter (inner / outer)	79.4 / 133.2	mm
Rotor diameter (inner / outer)	134.2 / 145	mm
Steel material	23PNX1200F	-
Air gap	0.5	mm
Stack length	9.6	mm
Magnet material	N52UH	-
Turns per layer	79	turns
Current density (continuous / maximum)	8.8 / 22.65	A_{rms}/mm^2
Rotation Speed (continuous / maximum)	1200 / 1600	RPM
Rated torque	3	Nm

FIGURE 8. The analysis periodic shape and design variables for target motor.

showed a 73.68 % success rate in 1,040 function calls and the ES showed a 92.92 % success rate in 2305 function calls. Lastly, with the third test function with 4 peaks, the AES showed a 99.26 % success rate in 315 function calls, while the NGA showed a 69.99 % success rate in 540 function calls and the ES showed an 86.09 % success rate in 1063 function calls. Finally, compared to the ES, the proposed algorithm demonstrates its superiority by respectively reducing the number of function calls (i.e., convergence speed) by 73.52%, 68.11%, and 70.37%, and respectively improving accuracy by 5.57%p, 6.11%p, and 13.17%p. And, compared to the NGA, the proposed algorithm demonstrates its superiority by respectively reducing the number of function calls by 43.63%, 29.33%, and 41.67%, and respectively improving accuracy by 18.42%p, 25.35%p, and 29.27%p.

TABLE 5. Design variables and ranges of the objective motor.

Variable	Range	Unit
Arc radius	5 ~ 14	mm
Alpha	0.5 ~ 2	mm

TABLE 6. Results of comparison with initial model and optimal models.

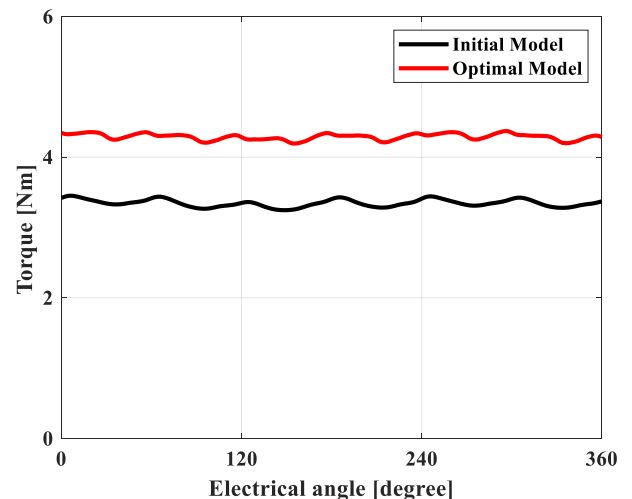| Model	Initial model	Case 1	Case 2	Case 3	Unit
Arc radius	5.60	12.35	12.28	13.71	mm
Alpha	1.87	0.52	0.50	0.64	mm
Average torque	3.28	4.27	4.24	4.29	Nm
Torque ripple	5.03	3.08	3.40	4.99	%
Objective function	1	0.67	0.72	0.71	-

FIGURE 9. Waveform comparison between the initial and optimal models of average torque.

IV. OPTIMAL DESIGN OF THE SPMSM FOR UAV
A. DESIGN OF THE SPMSM FOR UAV
The requirements for SPMSM for UAV driving are shown in Table 4. It is designed to achieve these specifications and selected as the initial model. However, looking at the results in Table 5, the torque achieves the rated torque, but it is judged that further reduction is still needed in terms of torque ripple. Therefore, an optimal design is performed based on the proposed algorithm.

The non-linear properties of the motor result in performance changes with even small changes in variable. For these reasons, it is very important to select the design variables. The model of the outer-rotor SPMSM is designed for high efficiency, light weight, and comfortable driving. Design variables, keeping slot area, are used in this paper, as shown in Fig. 8. The arc radius is the radius of the alpha arc facing the magnet and is not the distance from the center to the end of the motor. The arc radius affects the shape of the steel part

facing the magnets. When the arc radius is longer, the steel part is more convex; the shorter is the arc radius, the flatter is the steel part. At that time, the length of the air gap is fixed to reduce effects on the motor. Tables 4 shows the specifications of the SPMSM for UAV. The stacking length is 9.6 mm, and the dimension of motor is 134.2 mm. Concentrated winding is used to increase the space factor, and a natural cooling method is used. Table 5 shows the design variables and their ranges. The range of the arc radius is from 5 mm to 14 mm. and that of alpha is from 0.5 mm to 2 mm. J-MAG Designer, a commercial finite element analysis tool for analyzing the motor, for optimal design is used.

B. OPTIMAL DESIGN USING THE AES ALGORITHM

This paper verifies the validity of the algorithm by optimizing the motor for UAV using the proposed algorithm. The SPMSM for the UAV basically has two driving points at continuous and maximum. Among them, continuous driving point is sensitive to the noise and vibrations the most and need stable operation. Therefore, this paper optimizes in the condition of continuous driving point. While driving the motor, performance characteristics used as objective functions to optimally design motors for UAVs. Among them, torque and torque ripple affecting noise, vibration, and output power are determined as the objective functions for the characteristic of the UAV. The objective functions of the proposed algorithm are minimization of torque ripple to reduce noise and vibration during operation and maximization of average torque for high operation performance [8]. normalization to consider two objective variables. If only the FEA analysis is performed without normalization, the objective variable with a larger variation among torque and torque ripple is advantageous for improvement, but the objective variable with a smaller variation may not be improved. In order to prevent the problem caused by the size difference of some of these objective functions, normalization is performed and used into the weighted sums. The formula is as follow

$$\min f(x_i) = w_1 \frac{T_{avg,0}}{T_{avg}(x_i)} + w_2 \frac{T_{rip}(x_i)}{T_{rip,0}} \quad (7)$$

where $f(x_i)$ is the objective function, w_1, w_2 are the weight coefficients, and $T_{avg,0}$, $T_{rip,0}$ are torque average and torque ripple of the initial model. In this paper, average torque of the initial model exceeded the rated torque. Therefore, w_1, w_2 are determined as respectively 0.4, 0.6 to have more influence on the torque ripple.

As a result of performing the proposed algorithm, three of the best solutions are selected. Using load condition analysis, the three candidate models and the values of the initial model were performed and are shown in Table 6. First, in the initial model, the average torque was 3.28 Nm with a torque ripple of 5.03 %. The case 1 shows an average torque increase of 30.18 % and 38.77 % decrease in torque ripple.

And the case 2 and 3 show respectively an average torque increase of 29.27 % and 30.79 % and torque ripple decrease of 32.41 % and 0.80 %. Among them, the case 1, which is
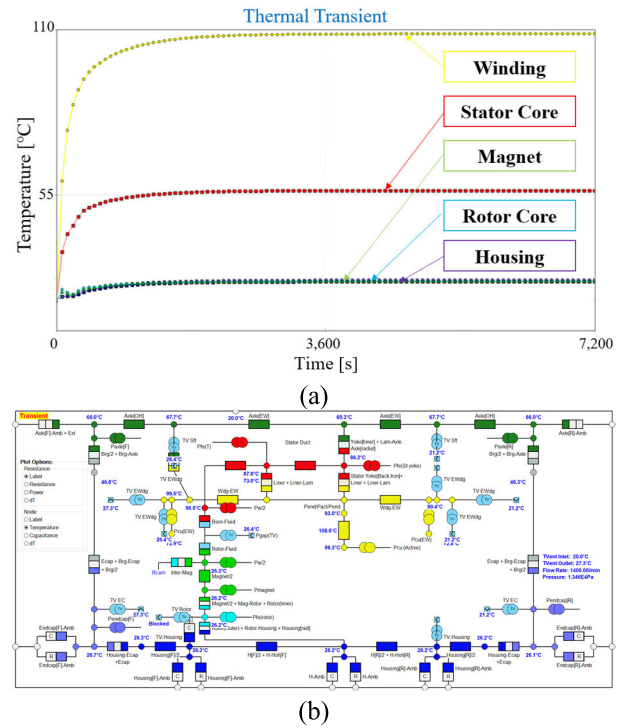

(a)

(b)

FIGURE 10. Results of thermal equivalent circuit analysis at the (a) thermal characteristic curve over time. (b) thermal equivalent circuits.

the best torque ripple improvement rate with similar average torque, is determined as the optimal model. In Fig. 9, the waveform of the torque of optimal model is compared with the initial model and show that optimal model is optimized from the initial model.

C. RELIABILITY VERIFICATION OF OPTIMAL MODEL

Generally, SPMSMs are more vulnerable to irreversible demagnetization compared with IPMSMs [40].

When performing the optimal design at high temperatures, the performance of the magnet may be deteriorated due to the irreversible demagnetization [41], [42]. Therefore, in this paper, to verify the stability of the magnet in such condition, after determining the maximum temperature through thermal analysis, irreversible demagnetization analysis is performed at the high temperature.

1) THERMAL EQUIVALENT CIRCUIT ANALYSIS

Setting the appropriate temperature condition is needed to analyze the irreversible demagnetization analysis. In this paper, to derive the maximum temperature of the optimal model, thermal equivalent circuit analysis is conducted. It was performed at the maximum driving point with the highest current, and the thermal equivalent circuit was constructed while generating heat source using the iron loss and copper loss [43]. The analysis was conducted for 2 hours at the maximum driving point. These processes are performed using Ansys Motor CAD. Fig. 11 shows results of thermal equivalent circuit analysis. As shown in Fig 11. (a), result of the maximum temperature is about 110 °C.
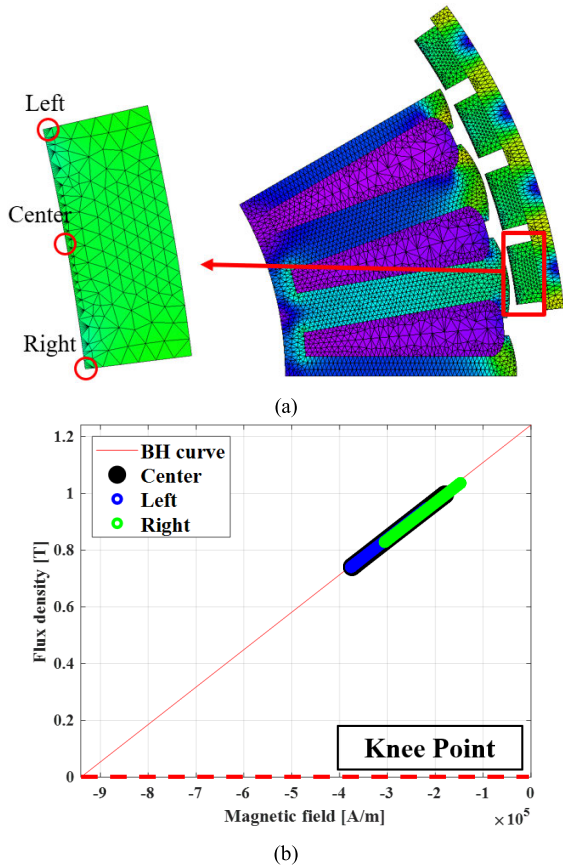
FIGURE 11. Vulnerable point of the magnet and result of irreversible demagnetization at vulnerable points at high temperature. (a) vulnerable point of the SPMSM. (b) result of irreversible demagnetization.

2) IRREVERSIBLE DEMAGNETIZTION ANALYSIS

It is essential to verify the performance of magnets at high temperatures. In this paper, irreversible demagnetization analysis of the motor is performed at 120 °C with about 10 % margin from 110 °C, which is derived by thermal equivalent circuit analysis, and a current phase angle of 90 °. The analysis of irreversible demagnetization is conducted in two methods.

The first method is to verify whether the operating point, which is the intersection of BH curve and load line of the motor, of the magnet's vulnerable points such as the center and edge of magnet [44] is formed above or below the knee point of the demagnetization curve with irreversible demagnetization characteristics [45], [46]. The second method is to compare back electromotive force before and after current of harsh condition applied and confirm by whether the reduction in back electromotive force occurs within 5 %. While considering the driving temperature and load characteristics of the motor, Fig. 12. (a) is shown vulnerable point of the SPMSM. In Fig. 12. (b), the operating points of each vulnerable point are shown above the knee point. Therefore, it is confirmed that irreversible demagnetization did not occur. And using second method on the same conditions, Fig. 11 is shown rate of reduction in back electromotive force before and after
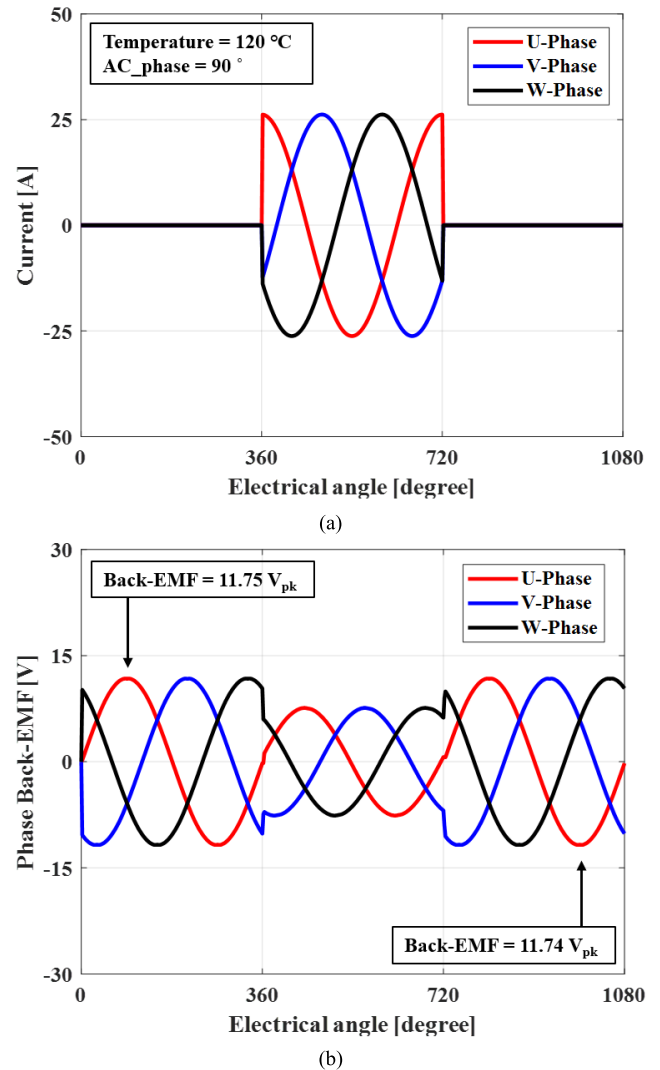

FIGURE 12. Result of the irreversible demagnetization analysis. (a) applied current. (b) comparison of no-load back-electromotive force with before and after current applied.

current applied. The magnitude of the no-load back electromotive force before the current is applied is 11.75 V_{pk}. And, after current, which has a current phase angle of 90 degrees, is applied, the magnitude of the no-load back electromotive force is 11.74 V_{pk}. Reduction rate of the back electromotive force is 0.085 %, therefore, it is confirmed that irreversible demagnetization did not occur. These results are verified the stability of the permanent magnets.

V. CONCLUSION

This study proposes a new algorithm, AES, that combines some method reducing the function calls and improving the convergence characteristic in the conventional ES. Using this algorithm for three test functions, not only the computation time was reduced but also the accuracy was increased than using the conventional ES and NGA. And then, when the AES was applied to the optimal design of the outer-rotor SPMSM, the output performance was improved while

increasing average torque and reducing torque ripple caused by noise and vibration. And using method to prove the stability of the motor, validity of proposed model is shown. The results of this study are expected to be widely applied to the multimodal optimization problem of various electrical machines utilizing FEM.

REFERENCES

[1] M. E. Antonio-Toledo, E. N. Sanchez, and A. Y. Alanis, "Robust neural decentralized control for a quadrotor UAV," in *Proc. Int. Joint Conf. Neural Netw. (IJCNN)*, Vancouver, BC, Canada, Jul. 2016, pp. 714–719.

[2] E. Fresk, G. Nikolakopoulos, and T. Gustafsson, "A generalized reduced-complexity inertial navigation system for unmanned aerial vehicles," *IEEE Trans. Control Syst. Technol.*, vol. 25, no. 1, pp. 192–207, Jan. 2017.

[3] J.-M. Ahn, J.-C. Son, and D.-K. Lim, "Optimal design of outer-rotor surface mounted permanent magnet synchronous motor for cogging torque reduction using territory particle swarm optimization," *J. Electr. Eng. Technol.*, vol. 16, no. 1, pp. 429–436, Jan. 2021.

[4] X. Xu and Y. Deng, "UAV power component—DC brushless motor design with merging adjacent-disturbances and integrated-dispatching pigeon-inspired optimization," *IEEE Trans. Magn.*, vol. 54, no. 8, pp. 1–7, Aug. 2018.

[5] C. Liu, J. Yu, and C. H. T. Lee, "A new electric magnetic-geared machine for electric unmanned aerial vehicles," *IEEE Trans. Magn.*, vol. 53, no. 11, pp. 1–6, Nov. 2017.

[6] S. Wang, Z. Lv, Y. Zhao, H. Yan, Y. Ren, L. Xiao, and G. Qiao, "Temperature field and heat load research for main propellant direct drive permanent magnet motor of unmanned aerial vehicle," in *Proc. 17th Int. Conf. Electr. Mach. Syst. (ICEMS)*, Hangzhou, China, Oct. 2014, pp. 2360–2364.

[7] P. Bogusz, M. Korkosz, A. Powrózek, J. Prokop, and P. Wygonik, "An analysis of properties of the BLDC motor for unmanned aerial vehicle hybrid drive," in *Proc. Int. Conf. Electr. Drives Power Electron. (EDPE)*, Tatranska Lomnica, Slovakia, Sep. 2015, pp. 458–464.

[8] W.-S. Jung, H.-K. Lee, Y.-K. Lee, S.-M. Kim, J.-I. Lee, and J.-Y. Choi, "Analysis and comparison of permanent magnet synchronous motors according to rotor type under the same design specifications," *Energies*, vol. 16, no. 3, p. 1306, Jan. 2023.

[9] C. He and T. Wu, "Analysis and design of surface permanent magnet synchronous motor and generator," *CES Trans. Electr. Mach. Syst.*, vol. 3, no. 1, pp. 94–100, Mar. 2019.

[10] S. S. R. Bonthu, Md. T. B. Tarek, and S. Choi, "Optimal torque ripple reduction technique for outer rotor permanent magnet synchronous reluctance motors," *IEEE Trans. Energy Convers.*, vol. 33, no. 3, pp. 1184–1192, Sep. 2018.

[11] N. Chen, S. L. Ho, and W. N. Fu, "Optimization of permanent magnet surface shapes of electric motors for minimization of cogging torque using FEM," *IEEE Trans. Magn.*, vol. 46, no. 6, pp. 2478–2481, Jun. 2010.

[12] Y.-R. Kang, J.-C. Son, and D.-K. Lim, "Optimal design of IPMSM for fuel cell electric vehicles using autotuning elliptical niching genetic algorithm," *IEEE Access*, vol. 8, pp. 117405–117412, 2020.

[13] C.-H. Wi and D.-K. Lim, "Tornado optimization with pattern search method for optimal design of IPMSM," *IEEE Trans. Magn.*, vol. 58, no. 2, pp. 1–4, Feb. 2022.

[14] J. Gao, L. Dai, and W. Zhang, "Improved genetic optimization algorithm with subdomain model for multi-objective optimal design of SPMSM," *CES Trans. Electr. Mach. Syst.*, vol. 2, no. 1, pp. 160–165, Mar. 2018.

[15] O. Aichholzer, F. Aurenhammer, B. Brandstatter, T. Ebner, H. Krasser, C. Magele, M. Muhlmann, and W. Renhart, "Evolution strategy and hierarchical clustering," *IEEE Trans. Magn.*, vol. 38, no. 2, pp. 1041–1044, Mar. 2002.

[16] J. Zhang, X. Yuan, Z. Zeng, and S. Amer, "Niching in as ES/EP context," in *Proc. Congr. Evol. Comput.*, vol. 2, 1999, pp. 1426–1433.

[17] H. J. Na and S.-J. Yoo, "PSO-based dynamic UAV positioning algorithm for sensing information acquisition in wireless sensor networks," *IEEE Access*, vol. 7, pp. 77499–77513, 2019.

[18] J. J. Jui and M. A. Ahmad, "A hybrid metaheuristic algorithm for identification of continuous-time Hammerstein systems," *Appl. Math. Model.*, vol. 95, pp. 339–360, Jul. 2021.

[19] X. Liu, G. Li, H. Yang, N. Zhang, L. Wang, and P. Shao, "Agricultural UAV trajectory planning by incorporating multi-mechanism improved grey wolf optimization algorithm," *Exp. Syst. Appl.*, vol. 233, Dec. 2023, Art. no. 120946.

[20] J. Zhou, W. Wang, J. Lu, and L. Liu, "Small unmanned helicopter modeling method based on a hybrid kernel function PSO-LSSVM," *J. Supercomput.*, vol. 79, no. 12, pp. 13889–13906, Aug. 2023.

[21] Y. Huang, T. Watanabe, M. Bando, and S. Hokamoto, "PSO algorithm parameter settings and optimal multi-rotor layout design," *Int. J. Sustain. Aviation*, vol. 8, no. 2, pp. 116–135, 2022.

[22] S. Yang, H. Wang, Y. Xu, Y. Guo, L. Pan, J. Zhang, X. Guo, D. Meng, and J. Wang, "A coupled simulated annealing and particle swarm optimization reliability-based design optimization strategy under hybrid uncertainties," *Mathematics*, vol. 11, no. 23, p. 4790, Nov. 2023.

[23] D. Meng, S. Yang, A. M. P. De Jesus, T. Fazeres-Ferradosa, and S.-P. Zhu, "A novel hybrid adaptive Kriging and water cycle algorithm for reliability-based design and optimization strategy: Application in offshore wind turbine monopile," *Comput. Methods Appl. Mech. Eng.*, vol. 412, Jul. 2023, Art. no. 116083.

[24] C. Lu, D. Teng, J.-Y. Chen, C.-W. Fei, and B. Keshtegar, "Adaptive vectorial surrogate modeling framework for multi-objective reliability estimation," *Rel. Eng. Syst. Saf.*, vol. 234, Jun. 2023, Art. no. 109148.

[25] D. Meng, H. Yang, S. Yang, Y. Zhang, A. M. P. D. Jesus, J. Correia, T. Fazeres-Ferradosa, W. Macek, R. Branco, and S.-P. Zhu, "Kriging-assisted hybrid reliability design and optimization of offshore wind turbine support structure based on a portfolio allocation strategy," *Ocean Eng.*, vol. 295, Mar. 2024, Art. no. 116842.

[26] D. Meng, S. Yang, A. M. P. D. Jesus, and S.-P. Zhu, "A novel Kriging-model-assisted reliability-based multidisciplinary design optimization strategy and its application in the offshore wind turbine tower," *Renew. Energy*, vol. 203, pp. 407–420, Feb. 2023.

[27] D. Teng, Y.-W. Feng, C. Lu, B. Keshtegar, and X.-F. Xue, "Generative adversarial surrogate modeling framework for aerospace engineering structural system reliability design," *Aerosp. Sci. Technol.*, vol. 144, Jan. 2024, Art. no. 108781.

[28] M. Fatehi, A. Toloei, E. Zio, S. T. A. Niaki, and B. Keshtegar, "Robust optimization of the design of monopropellant propulsion control systems using an advanced teaching-learning-based optimization method," *Eng. Appl. Artif. Intell.*, vol. 126, pp. 106–778, Nov. 2023.

[29] K.-Y. Yoon and K.-Y. Hwang, "Optimal design of spoke-type IPM motor allowing irreversible demagnetization to minimize PM weight," *IEEE Access*, vol. 9, pp. 65721–65729, 2021.

[30] B. Son, J.-S. Kim, J.-W. Kim, Y.-J. Kim, and S.-Y. Jung, "Adaptive particle swarm optimization based on kernel support vector machine for optimal design of synchronous reluctance motor," *IEEE Trans. Magn.*, vol. 55, no. 6, pp. 1–5, Jun. 2019.

[31] H. Yan and X. Zhang, "Design and optimization of a novel supersonic rocket with small caliber," *J. Ind. Manag. Optim.*, vol. 19, no. 5, pp. 3794–3818, 2023.

[32] O. Takahashi and S. Kobayashi, "An adaptive neighboring search using crossover-like mutation for multi modal function optimization," in *Proc. IEEE Int. Conf. Syst., Man Cybern. E-Syst. E-Man Cybern. Cyberspace*, 2001, pp. 261–267.

[33] D.-H. Cho, J.-K. Kim, H.-K. Jung, and C.-G. Lee, "Optimal design of permanent-magnet motor using autotuning niching genetic algorithm," *IEEE Trans. Magn.*, vol. 39, no. 3, pp. 1265–1268, May 2003.

[34] C.-H. Im, H.-K. Kim, H.-K. Jung, and K. Choi, "A novel algorithm for multimodal function optimization based on evolution strategy," *IEEE Trans. Magn.*, vol. 40, no. 2, pp. 1224–1227, Mar. 2004.

[35] K.-T. Kim, S.-H. Kwon, J.-H. Ko, and H.-S. Kim, "An optimal design of a 19.05 GHz high gain 4X4 array antenna using the evolution strategy," *Trans. Korean Inst. Electr. Eng.*, vol. 60, no. 4, pp. 811–816, Apr. 2011.

[36] T. Back, *Evolutionary Algorithms in Theory and Practice*. Oxford, U.K. Oxford Univ. Press, 1996.

[37] J.-H. Ko, K.-T. Kim, D.-H. Kim, H.-B. Lee, and H.-S. Kim, "A practical approach to robust design of a RFID triple-band PIFA structure," *IEEE Trans. Magn.*, vol. 46, no. 8, pp. 3333–3336, Aug. 2010.

[38] H.-J. Park, H.-K. Yeo, S.-Y. Jung, T.-K. Chung, J.-S. Ro, and H.-K. Jung, "A robust multimodal optimization algorithm based on a sub-division surrogate model and an improved sampling method," *IEEE Trans. Magn.*, vol. 54, no. 3, pp. 1–4, Mar. 2018.

[39] T.-H. Lee, Y.-R. Kang, J.-C. Son, and D.-K. Lim, "Optimized design of permanent magnet assisted synchronous reluctance motor using oriented auto-tuning niching algorithm," *J. Electr. Eng. Technol.*, vol. 16, no. 3, pp. 1495–1503, May 2021.

[40] L. Wu, Y. Du, Z. Chen, Y. Guo, H. Wen, and Y. Fang, "Influence of load characteristics on three-phase short circuit and demagnetization of surface-mounted PM synchronous motor," *IEEE Trans. Ind. Appl.*, vol. 56, no. 3, pp. 2427–2440, May 2020.

[41] G.-H. Kang, J. Hur, H. Nam, J.-P. Hong, and G.-T. Kim, "Analysis of irreversible magnet demagnetization in line-start motors based on the finite-element method," *IEEE Trans. Magn.*, vol. 39, no. 3, pp. 1488–1491, May 2003.

[42] S. Ruoho, J. Kolehmainen, J. Ikaheimo, and A. Arkkio, "Interdependence of demagnetization, loading, and temperature rise in a permanent-magnet synchronous motor," *IEEE Trans. Magn.*, vol. 46, no. 3, pp. 949–953, Mar. 2010.

[43] M.-S. Kwon and D.-K. Lim, "A study on the optimal design of PMa-SynRM for electric vehicles combining random forest and genetic algorithm," *IEEE Access*, vol. 11, pp. 52357–52369, 2023.

[44] G. Choi and T. M. Jahns, "Post-demagnetization characteristics of permanent magnet synchronous machines," in *Proc. IEEE Energy Convers. Congr. Expo.*, Montreal, QC, Canada, Sep. 2015, pp. 1781–1788.

[45] P. Peng, H. Xiong, J. Zhang, W. Li, F. Leonardi, C. Rong, M. W. Degner, F. Liang, and L. Zhu, "Effects of external field orientation on permanent magnet demagnetization," *IEEE Trans. Ind. Appl.*, vol. 53, no. 4, pp. 3438–3446, Jul. 2017.

[46] P. Zhou, D. Lin, Y. Xiao, N. Lambert, and M. A. Rahman, "Temperature-dependent demagnetization model of permanent magnets for finite element analysis," *IEEE Trans. Magn.*, vol. 48, no. 2, pp. 1031–1034, Feb. 2012.

TAE-HO OH received the M.S. degree in electronic engineering from Kyungpook National University, Daegu, South Korea, in 2018.

He is currently the Manager of the Research and Development Center, Advanced Control Development Team 1, DN Solutions. His research interest includes servo and spindle motor design in machine tools.

DONG-KUK LIM (Member, IEEE) received the B.S. degree in electrical engineering from Dongguk University, Seoul, South Korea, in 2010, and the Ph.D. degree in electrical engineering from Seoul National University, Seoul, in 2017, through the combined master's and Ph.D. program.

In 2017, he was a Senior Research Engineer with the Electrical Power Engineering Team, Hyundai Mobis Company, South Korea. He is currently an Associate Professor with the School of Electrical Engineering, University of Ulsan, South Korea. His research interest includes analysis and optimal design of electrical machines.

JUNG-WOO KIM received the B.S. degree in electrical engineering from the School of Electrical Engineering, University of Ulsan, South Korea, in 2023, where he is currently pursuing the M.S. degree.

His research interest includes analysis and optimal design of electrical machines.

CHUL YUN received the Ph.D. degree in electronic engineering from Kyungpook National University, Daegu, South Korea, in 2018.

He is currently the Senior Manager of the Research and Development Center, Advanced Control Development Team 1, DN Solutions. His research interests include servo and spindle motor control, and power conversion in machine tools.

JIN-HWAN LEE received the B.S. and Ph.D. degrees in electronic and electrical engineering from Sungkyunkwan University, Suwon-si, South Korea, in 2013 and 2018, respectively.

He was a Senior Research Engineer with the Research and Development Division, Hyundai Transys. He is currently an Assistant Professor with the Department of Electrical Engineering, Chonnam National University. His research interests include numerical analysis and design optimization of electric machines, development of optimization algorithm customized for electric machines, and development on analysis precision improvement technique of electric machines.

● ● ●